Proceedings of ASME Turbo Expo 2011
GT2011
June 6-10, 2011, Vancouver, British Columbia, Canada

GT2011-46457

NUMERICAL INVESTIGATION OF A HIGHLY LOADED AXIAL COMPRESSOR STAGE WITH INLET DISTORTIONS

Andreas Lesser*, Jens Iseler, Reinhard Niehuis
Institute of Jet Propulsion
University of the Federal Armed Forces Munich
85577 Neubiberg
Germany
Email: andreas.lesser@unibw.de

ABSTRACT

This paper deals with the numerical flow-simulation of a transonic compressor stage, which has been investigated for baseline as well as distorted inflow conditions at the Institute of Propulsion Technology of the DLR in Cologne (Dunker [1] and Lecht [2]). The inlet distortions are generated in the experiment upstream of the compressor stage by non-rotating steel bars, while in the numerical calculations the total pressure and inflow angle distribution measured downstream of the bars are taken as inflow boundary conditions. The circumferential extent of the generated total pressure and inflow angle distortion is 120 degrees. Numerical simulations were performed for uniform inflow conditions at 85% and 100% rotational speed. For disturbed inflow conditions, a full-annulus calculation has been carried out for an operational point at peak efficiency. The object of the investigations is to validate the flow solver for compressor flow with distorted inflow. The results from time-averaged numerical and experimental data are compared extensively. The experimental trends are qualitativly and in the most part also quantitativly well reproduced in the numerical calculations.

NOMENCLATURE

p static Pressure
T Temperature
P_t total pressure
T_t total temperature
α radial flow angle

INTRODUCTION

In order to increase safety and efficiency and decrease costs during the design and development process of modern aircraft, highly efficient and accurate design tools are necessary. One demand on these tools is to predict the flow behavior on the aircraft fuselage and its wings as well as inside of the jet engine for an entire flight mission. To achieve this aim the flow physics have to be simulated correctly and therefore the interaction of the inner jet engine flow and the outer flow around the aircraft has to be taken into account. An accurate simulation is crucial for situations where high aerodynamic loads are present. Critical phases occur amongst others at take-off or flight through an area with strong crosswind, where highly turbulent air with both spacial and temporal variations may dominate the inflow of the jet engine. These intake distortions increase the risk of compression system instabilities and loss of efficiency. Inlet distortions may be composed of total pressure-, angle-, and total temperature distortions, depending on the particular configuration. All three disturbances cause a reduction of the stable operation range. Despite many experimental investigations, there is still a high demand for research in the field of inlet distortions. A good overview of the effects of intake distortions is given by Longley and Greitzer [3], as well as by Cousins [4]. Experimental investigations were carried out by Schmidt et al. [5], Peters et al. [6] [7], Reuss [6] and Wadia et al. [8], [9]. In order to predict accurately the creation

*Address all correspondence to this author.

and the migration of the inlet disturbances and their impact on the compressor, the aerodynamics in front of the engine and the flow into the jet engine have to be simulated simultaneously. At present, most of the numerical methods are specialized either for inner or for outer aerodynamics. One possibility to solve this problem is to couple two codes: one specialized for inner and the other for outer flow dynamics. This strategy is pursued by members of the DFG (German Research Foundation) research project FOR 1066, where two DLR codes TAU and TRACE are coupled. In this paper validation tests of the TRACE-code are presented with the focus on inlet distortion and its effect on compressor performance. These validation tests refer to a data set of a transonic compressor stage, which was experimentally investigated for uniform [10], [1] and disturbed [2] inflow conditions at the DLR's Institute of Propulsion Technology in Cologne (DLR AT). The speed line characteristics are used to gauge the overall performance of the machine and to evaluate the accuracy of simulations of the compressor in general. The experimental data collected by Lecht [2] are the total pressure ratio, total temperature ratio and flow angles on various axial cross sections of the compressor stage. One consequence of distorted inflow is a shift in the surge line and hence a decreasing operational range.

TEST CASE AND TEST ROTOR

The compressor stage under investigation in this study is a transonic high-pressure compressor, operated at the DLR AT. The experimental setup is shown in Figure 1. It was designed for a spool speed of 20260 RPM with a total pressure ratio of 1.51 at an equivalent mass flow of 17.3 kg/s under standard reference conditions (288 K and 101325 Pa). The rotor diameter is 398 mm with a hub-to-tip ratio of 0.5 and a maximum blade tip speed of 424 m/s. Overall, 28 blades with MCA profile and an average chord length of 50 mm were used.

Two different stator rows were used, depending on whether disturbed or undisturbed inflow conditions were applied: For uniform inflow conditions, the blade row consists of 60 blades with NACA-65-profiles, while for distorted inflow conditions 72 blades of the same profile were used. For the configuration with 28 rotor- and 60 stator blades, detailed temperature and pressure measurements as well as Laser2Focus measurements are available. For the second configuration, detailed measurements of temperature, pressure, and flow direction exist only with disturbed inflow conditions. For all measurements there are no available data for turbulent intensity or turbulent length scale. In Table 1, the main parameters of the compressor are summarized. The inlet distortions were generated upstream of the compressor stage by a wake generator with non-rotating steel bars. The circumferential extent of these distortions was either 60 or 120 degrees. However, most of the published experimental data refers to the 120 degree-distortion.

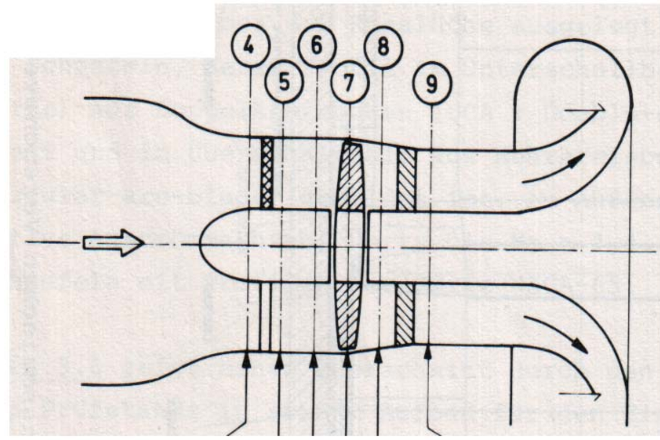

FIGURE 1. TRANSONIC COMPRESSORE STAGE TEST RIG WITH MEASUREMENT PLANES, [2]

NUMERICAL PROCEDURE

Solver

All numerical results presented in this paper have been carried out using the flow solver TRACE developed by DLR AT in collaboration with MTU Aero Engines. The code solves the unsteady Reynolds averaged Navier-Stokes equations with a finite volume approach and is optimized for the computation of internal flows in turbomachines. All convective fluxes are discretized using the TVD upwind scheme by Roe [11], which is combined with a MUSCL extrapolation scheme to gain second order accuracy in space. On the other hand all diffusive fluxes are discretized using a second order central differencing scheme. For all steady state calculations presented in this study a time marching technique with an implicit predictor corrector scheme has been used. The dual time stepping approach used for the unsteady calculations utilizes an Euler implicit scheme within the pseudo-time level while a second order accurate Crank-Nicolson scheme is incorporated for physical time integration. The resulting linear system of equations is iteratively solved by a symmetric Gauss-Seidel relaxation scheme. A fully conservative and time-accurate coupling between moving and non-moving grid blocks is accomplished by a patched-cell algorithm [16]. Furthermore non-reflecting inflow and outflow boundary conditions are implemented. Turbulent flow is taken into account by using the Wilcox [12] k-ω turbulence model which is extended by a time scale bound by Durbin and Peterson-Reif [13] in order to avoid an unrealistic production of turbulence near stagnation points. For more detailed information about TRACE refer to Kožulović et al. [14] [15] , Yang et al. [16] [17], Nürnberger [18] and Eulitz [19].

TABLE 1. TRANSONIC COMPRESSURE STAGE AERODYNAMIC DESIGN PARAMETERS

Rotor speed at 100 % speed	20260 rpm
Rotor blade number	28
Mass flow rate	17.3 $\frac{kg}{s}$
Tip speed at 100 % speed	424 $\frac{m}{s}$
Total pressure ratio	1.5
Hub- tip ratio	0.5
Tip clearance	0.3 mm 0.3 % blade height 0.51 % chord length
Homogen. inflow cond. (Config. 1)	
Stator vane number	60
Profile	NACA65/60
Average chord length	30mm
Inhomogen. inflow cond. (Config. 2)	
Stator vane number	72
Profile	NACA65/60
Average chord length	22mm

Grid and Simulations

Four different types of numerical simulations were performed: Steady-state simulations for a one rotor and one stator blade passage, unsteady simulations for a configuration of one rotor blade passage and two stator blade passages as well as steady and unsteady simulation for the entire compressor stage. The first two simulation types were conducted with uniform inflow conditions. For steady runs, the mixing plane concept was applied. Here, the same uniform flow condition in all rotor and stator blade passages is assumed. In the absence of inlet distortion, a single passage caculation is a good approximation of the full annulus flow. The unsteady simulations were undertaken using the scaling technique, such that the number of rotor and stator blades must have a integer ratio. Thus, the stator geometry of configuration 1 had to be scaled down from 60 to 56 blades. Applying a grid with one rotor and two stator passages, results in a one-to-one match at the interface. The last two simulation types refer to distorted inflow conditions (configuration 2). Here no simplifications can be made and all 28 rotor and 72 stator passages have to be taken into account.

The simulations for uniform inflow conditions were conducted with a computational grid which was designed in order to accurately simulate flow phenomena like the tip leakage, blade row interactions, and shock-boundary layer interaction. The boundary layers on the blade surfaces are resolved with more than 20 elements in the wall normal direction. Seven elements in the radial and 155 elements in the axial direction are used for the tip gap. The grid for the axial gap between the rotor trailing edge and the stator leading edge consists of 51 elements in the axial direction, which permits an accurate simulation of the wake flow. Altogether the grid for the unsteady simulations with one blade and two vane passages contains about 1.2 million grid points.

In order to accurately predict the boundary layer development and the behaviour of the tip leakage vortex, the resolution of the grid was maintained from the single passage calculations, for flow-simulations with distorted inflow conditions. Therefore the computational grid consists of 766 structured blocks and more than 50 million grid points.

For unsteady runs, the governing time dimension has to be highly discretised in order to predict accurately the transient nature of the tip leakage flow and wake flow. This time dimension is related to the blade passing frequency. Overall 512 physical time steps were used to resolve this passing frequency. A converged unsteady flow simulation of the blade passage was obtained after 8 blade passing periods.

Boundary Conditions

For all walls viscous wall boundary treatment is used. The maximum y+ values are lower than 1.5 where low Reynolds treatment was used (blade walls) and about 30 where wall functions were used (hub and tip walls). At the exit plane of the compressor, equilibrium of the static pressure was prescribed. The treatment of the inlet boundary condition has to be adapted, hence the inlet boundary condition was used to prescribe the inlet distortion. A nonreflecting Giles [20] inlet boundary condition was modified to read in a 2D inlet plane for total pressure, total temperature and the inflow angle. Since experimental data is only available for midspan, the distortion is assumed to be constant in radial direction and varies only in circumferencial direction (see Figure 2).

Most of the experimental data was collected for a distortion of 120°extent, hence the 120°distortion was used for the simulations. The measured total pressure and inflow angle distributions behind the distortion generator are used as input for the inlet boundary condition of the numeric simulation. The measurement plane, and consequently the simulation inlet plane, is 50 mm upstream of the compressore stage. For the simulation, the input was smoothed somewhat for numerical reasons. Both measured and prescribed circumferencial total pressure and inflow angle distributions for 100% rotation speed at midspan are shown in Figure 3.

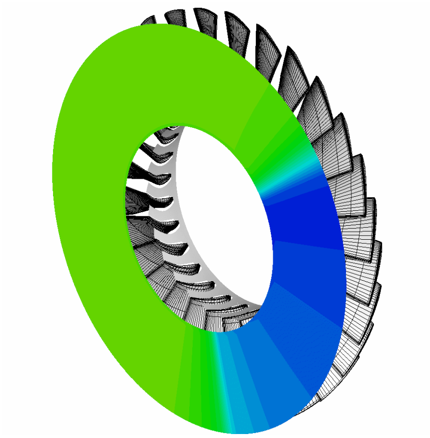

FIGURE 2. INLET PLANE WITH QUALITATIVE DISTORTION DISTRIBUTION

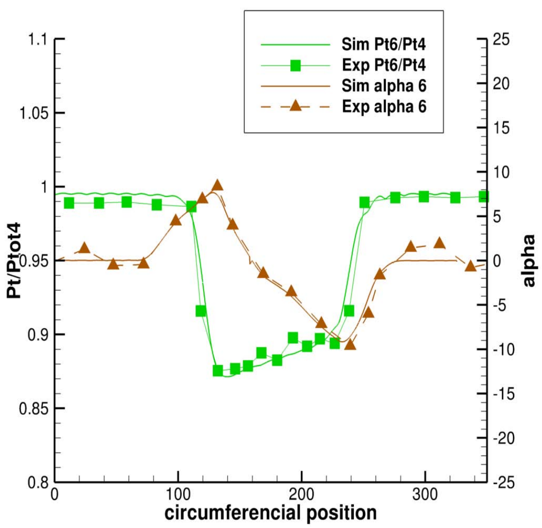

FIGURE 3. MEASURED AND PRESCRIBED INLET DISTORTION

RESULTS OF SINGLE PASSAFGE SIMULATIONS

In the first part of the investigation, steady and unsteady simulations were performed for uniform inflow conditions using the periodic boundary technique. The numerical investigations were conducted for the configuration 1, with 28 blades and due to domain scaling 56 vanes. Figure 4 displays the radial profile of the total temperature at 100% rotational speed near peak efficiency and near stall downstream of the stator row. Steady as well as time-averaged unsteady numerical data are plotted. The temperature distributions show a generally good agreement, particularly between 80% and 100% span. The maximum deviation of temperature rise is 10%. This difference occurs between 20% and 80% and is possibly due to the lack of a transition model. This assumption is supported by experiences of the authors with other transonic compressor calculations at the same Reynolds number of about 3 Million. The temperature plots show that steady and time-averaged unsteady numerical data are nearly the same. Obviously, the unsteadiness of the rotor stator interaction plays only a minor role at design speed.

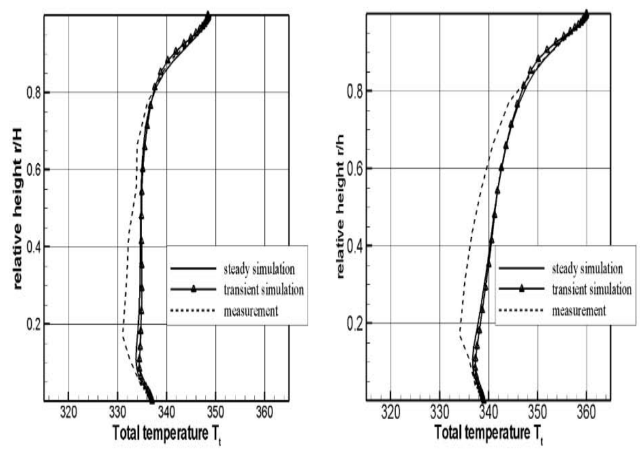

FIGURE 4. MEASURED AND PREDICTED TEMPERATURE PROFILES AT DESIGN CONDITIONS MIDCHANNEL AT STATOR EXIT, AT PEAK EFFICIENCY (LEFT) AND NEAR STALL (RIGHT)

The following two Figures display measured and simulated Mach number distributions at 100% rotational speed. Figure 5 shows the Mach number distribution for design condition, Figure 6 refers to flow conditions at high aerodynamic load. For both operating points, the time-averaged numerical data and the experimental data (acquired using the L2F-technique) show good agreement. The extent of the Prandtl-Meyer expansion, position and shape of the passage shock waves and Mach number levels for the whole rotor passage are well predicted. At design condition, both plots exhibit an oblique passage shock wave followed by a normal shock wave. Near instability onset, numerical and experimental data reveal a significant expansion on the suction side with Mach number values higher than 1.4. Furthermore, a detached normal shock has developed. Due to a significant shock-boundary layer interaction, a rapid growth of the boundary layer can be seen downstream of the shock position. Near

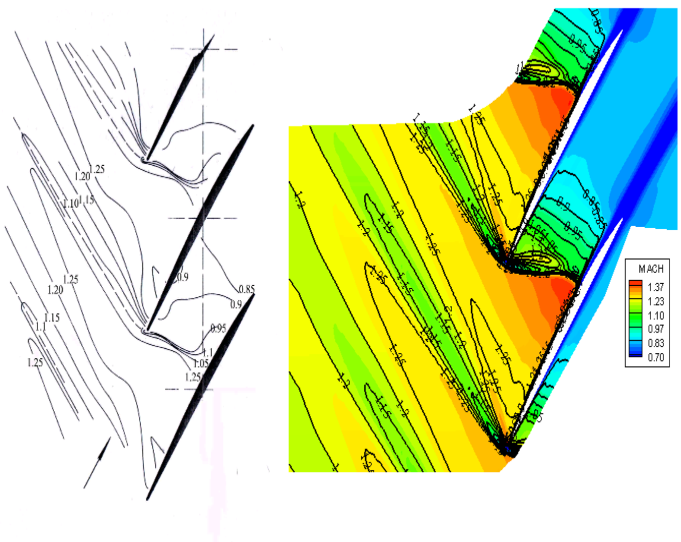

FIGURE 5. MEASURED (LEFT)AND SIMULATED MACH NUMBER DISTRIBUTION AT 69% SPAN AT PEAK EFFICIENCY AND 100% ROTATIONAL SPEED;

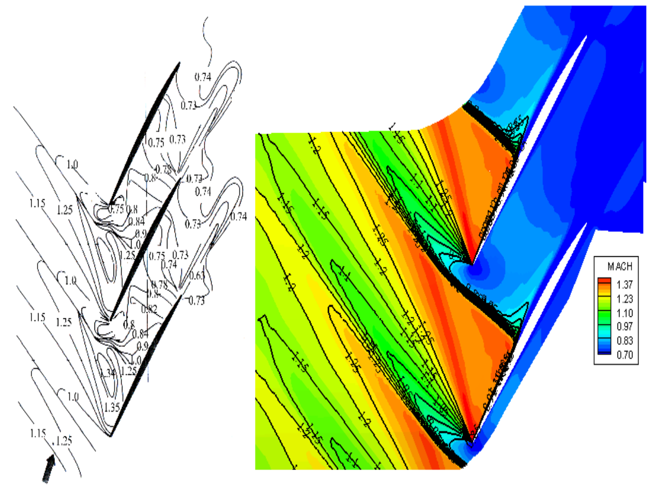

FIGURE 6. MEASURED (LEFT)AND SIMULATED MACH NUMBER DISTRIBUTION AT 69% SPAN NEAR STALL AND 100% ROTATIONAL SPEED;

the rotor tip, the boundary layer growth is underestimated by the simulation for high aerodynamic load. Nonetheless, a qualitative good overall prediction of the flow behaviour in the rotor section is achieved.

With the experience gained in the first part of the project, further simulations were performed for the second compressor configuration with 72 instead of 60 vanes. Since the geometry of the blades is identical, the stage geometry could be adjusted relatively easily. Steady simulations for one blade passage and uniform inflow conditions were carried out as a first step. This was done in order to compare the predicted and measured performance offset caused by the disturbed inflow.

Figure 7 shows the speedline of the compressor at 85% rotational speed as calculated from numerical and experimental data. The plot contains performance values for several operating points between peak efficiency and instability onset. Efficiency and total pressure ratio are normalised with their respective values at peak efficiency. Overall, a similar behaviour with a decreasing mass flow rate can be found. As the performance data represent the only available experimental data without inlet distortions, a more detailed analysis cannot be performed.

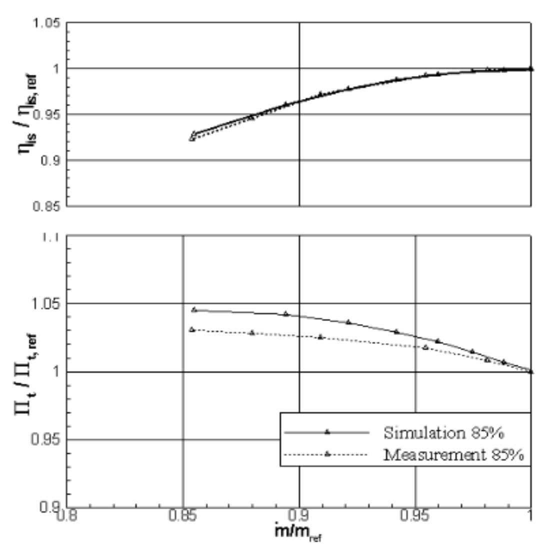

FIGURE 7. PERFORMANCE MAP FOR THE 85% CHARACTERISTIC, CONFIGUTRATION 2

Results of the simulations with distorted inlet

Due to limited computational ressources, only one operating point was simulated so far. The 85% characteristic was preferred, since more experimental data is available for this speedline. Measured and simulated inflow conditions are plotted in

Figure 3. At midspan, the extent of the total pressure distortion is almost 120°degrees and the pressure loss is up to 13%. Moreover, a variation of the inflow angle can also be seen. To validate the global flow behavior Figure 8 shows the measured pressure rise characteristics of the compressor stage at 85% of design rotor speed with distorted inflow. The comparison of the operating point displays global flow features and is hence a strong indication if the numerical simulation captures the general behavior. The operating point for peak efficiency is in good agreement with the measurement.

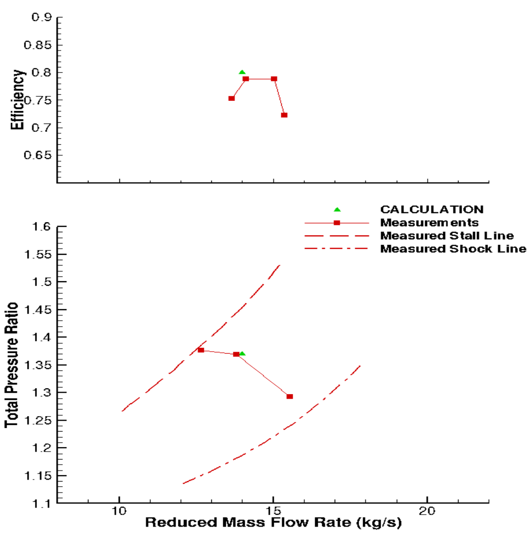

FIGURE 8. OPERATING POINT WITH DISTORTED INFLOW

Having confirmed that the global nature of the flow is correctly captured, the results can be discussed in more detail. Experimental data is available for three axial locations. In Figure 1 the measurement planes are shown and all indices refer to this nomenclature. For plane 6, which represents the distorted inflow plane upstream of the rotor, and for plane 9, which represents the outflow plane, only static and total pressures at midspan were measured in the experiment. For this reason the main focus will be on midspan data, especially since the inflow distortion was modelled only from midspan data as discussed previously. The circumferencial distribution between rotor and stator of total temperature, total pressure and the flow angle is also available for 25% and 75% span. Comparison of numerical and experimental data for these radial positions will be shown subsequently.

In Figure 9, the circumferential total and static pressure distribution for 50% span in the inlet plane are plotted. The total pressure in the simulation is fixed by the inflow boundary condition, while the static pressure is calculated. The global trend is

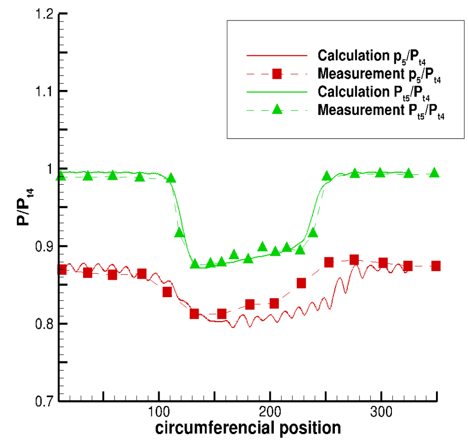

FIGURE 9. CIRCUMFERENCIAL TOTAL AND STATIC PRESSURE DISTRIBUTION, INLET PLANE

quantitativly and qualitativly in good agreement. The deviation of the static pressure caculated numerically is stronger between 220°and 260°than the deviation seen in the undistorted cases.

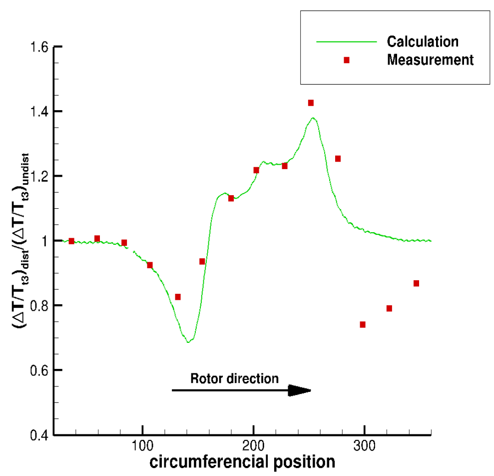

FIGURE 10. CIRCUMFERENCIAL TOTAL TEMPERATURE INCREASE DISTRIBUTION BETWEEN ROTOR AND STATOR, 50% SPAN, (Plane 8)

Between rotor and stator the measured and calculated results show a constant offset of less than 5 %, therefore to facilitate the comparison of the trends the flow quantities are referenced to undistorted flow. The circumferencial total temperature increase,

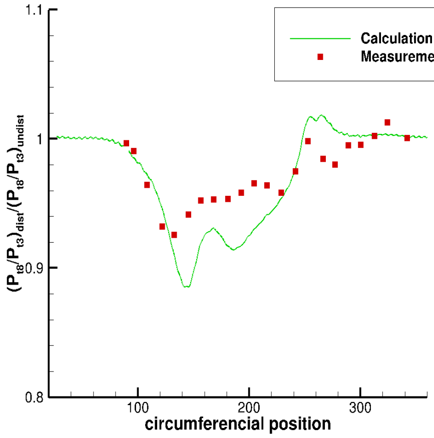

FIGURE 11. CIRCUMFERENCIAL TOTAL PRESSURE INCREASE DISTRIBUTION BETWEEN ROTOR AND STATOR, 50% SPAN, (Plane 8)

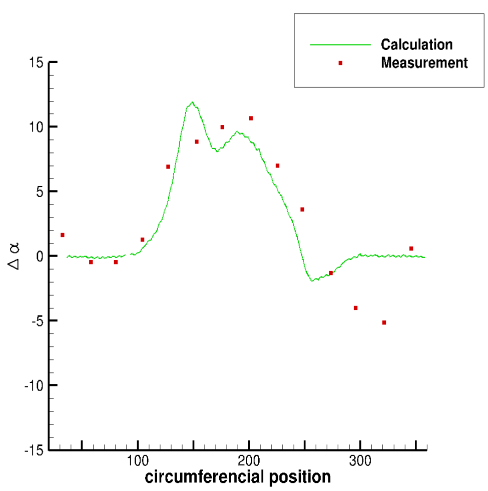

FIGURE 12. CIRCUMFERENCIAL FLOW ANGLE DISTRIBUTION BETWEEN ROTOR AND STATOR, 50% SPAN, (Plane 8)

total pressure increase and flow angle distribution are plotted in Figures 10 - 12. For the exit plane downstream of the stator only the total pressure increase distribution was measured at midspan, which can be seen in Figure 13. For all quantities the trend is reproduced for the most part reasonably well. Especially the total temperature increase during the distortion is reproduced. The total temperature increase reflects the specific energy addition. The trend is due to the interaction of the flow angle and total pressure deviation. The angle variation produces a co-spin for

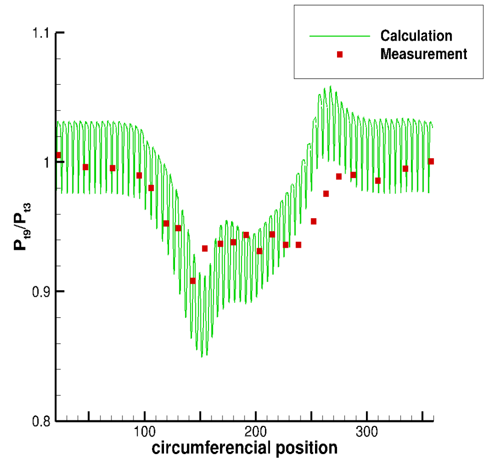

FIGURE 13. CIRCUMFERENCIAL TOTAL PRESSURE INCREASE DISTRIBUTION AFTER THE STATOR, 50% SPAN, (Plane 9)

the passing rotor blade in the first part of the distorted area and at approximately 300°where the algebraic sign changes a counter-spin. This affects the variation due to the total temperature increase. The rotor transfers less specific energy to the flow where loading is reduced and more where it is highly loaded. None of the calculated profiles matches the experiment from 280°to 340°circumferencial position, where experimetal results for total temperature and flow angle show a high gradient.

A closer look at the axial evolution of the total pressure increase shows, that the trend is reproduced in general well, however there are some deviations, too. For Planes 8 (Fig. 11) and 9 (Fig. 13), it can be seen that the slope of the decrease at 100°is well predicted, however the numerical calculation overestimates the entire decrease. The increase of total pressure in the simulation is more rapid but shows saddle points, like the experiment. At plane 9 (Fig. 13), the measured values of P_{t9} never seriously exceed P_{t3}, whereas this is the case for the numerical values.

The numerical results for total pressure and temperature combine with the $\Delta\alpha$ distribution between rotor and stator, plane 8, (Fig. 12). The slope are in good agreement, however the peaks are overpredicted at about 100°and underpredicted from 280°and 340°circumferencial position and the extent of the distortion in the numerical results is smaller than in the measurement.

As the part between 280°and 340°differs in all simulations from the measurements, it has to be discussed in detail. In the experimental results, the total temperature increase distribution (Figure 10) shows a depression between 280°- 340°, which is stronger than the first one between 100°- 150°and not reproduced by the numerical results. As the total temperature increase depicts the total energy addition this implies that in this part the rotor adds less energy to the fluid, although the inflow conditions for this part leads to a higher loaded blade. A higher loaded blade results in higher energy addition at least if the losses due to flow separation are not dominant. If significant flow separation occurs, the losses increase and hence the energy addition would decrease dramatically. Also the angle distribution is an indication of significant flow separation. The main source for angle deflection behind the rotor is the axial velocity distribution because of the total pressure distortion. This correlation can be seen in the simulated angle and total pressure distributions Figure 11 and 12. Where the total pressure is low also the axial flow component is low and therefore the magnitude of α increase in the velocity triangle. The high negative values in the part between between 280°- 340°of the measured angle distribution, in combination with the measured total pressure distribution show that the high negative values of the angle deviation occurs in an area where the total pressure distortion is quite small. These two facts suggest that massive flow separation occurs for this inflow conditions. For the correct reproduction of the flow separation, a transition model is required in the numerical calculation. All boundaries of the full annulus calculation were modeled as fully turbulent, because of limited computational resources. Hence transition effects can not be reproduced. To check the influence of the transition on the flow from 280°to 340°circumferencial position, single passage calculations have been carried out with and without a transition model. A γ-Re_θ [21] transition model, which is incorporated into the k-ω turbulence model was used to model transitional effects. The model accounts for several modes of transition that are dominant in turbomachinery flows, namely natural, bypass, separation induced and wake induced transition (cf. [22]). The conditions for the sector where the differences occur were taken as boundary conditions. Stable converging results for these conditions only developed for fully turbulent calculations. In order to get stable results with an active transition model, the static back pressure had to be reduced. The instability of the calculation with transition model is an indication that the flow behaviour depends on transitional effects and that significant flow separation occurs. Therefore it is most likely that the compressor operates in the sector from 280°to 340°beyond the stability boundary. This condition occurs if there is enough of the annulus operating on the stable side to maintain overall stability [3]. The single passage calculation with transition model is apparently better able to predict instabilities with the given flow conditions than full turbulent calculations. Hence it is most likely that the use of a transition model is able to reduce the gap between measurement and calculation.

Also the general overprediction of the decrease of the total pressure is likely due to turbulence modelling. For the use of eddy viscosity models like the Wilcox k-ω, model isotropic turbulence is assumed. Tests of Lecht [2] with the bar grid show that the mixing of the unsteady wake structures behind the bars is not complete even at the rotor trailing edge. So the assumption of isotropy turbulence is only somewhat valid. There is no possibility to take anisotropy into account because there is no experimental data and it would demand superior turbulence models, which would increase the computational effort immensely. Therefore, with the turbulence model used here, the momentum exchange between distorted and undistorted flow is most likely underpredicted. This results in a slower mix out of the total pressure distortion, in the numerical simulations.

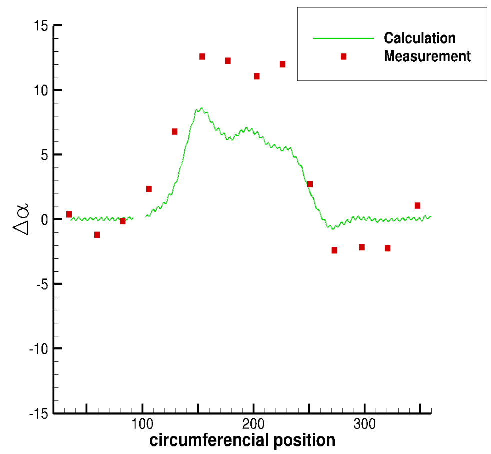

FIGURE 14. CIRCUMFERENCIAL FLOW ANGLE DISTRIBUTION BETWEEN ROTOR AND STATOR, 25% SPAN, (Plane 8)

Different spanwise positions are also considered. In Figures 15 and 14, the $\Delta\alpha$ distribution at 25% and 75% span are shown. The result for 75% span is quite similar to that for midspan, in terms of the well predicted trend and the negative overshoot in the part between 280°and 340°. In contrast to the midspan result the whole deflection is underpredicted. At 25% the underprediction is worse. The trend is still reproduced, but the amplitude is low. For the total temperature, Figures 16 and 17 show the comparison between simulation and experiment. In contrast to the flow angle distribution, the total temperature distribution shows a very good agreement at 25% and 75%, except between 280°and 340°. The reproduction of the total pressure at 75% span in Figure 18 shows the same trend as for midspan. The general trend is similar but the amplitude is overpredicted. Lecht [2] points out that in the experimental results, the total pressure distortion is mixing out stronger in radial direction, yet this trend is only weakly reproduced by the simulation. For 25% span the extent of the distortion is reproduced in spite of the fluctuation that is shown in the exprimental data between 100°and 200°. For the results at different spanwise positions one important shortcoming in the numerical setup is, that there is only midspan data of

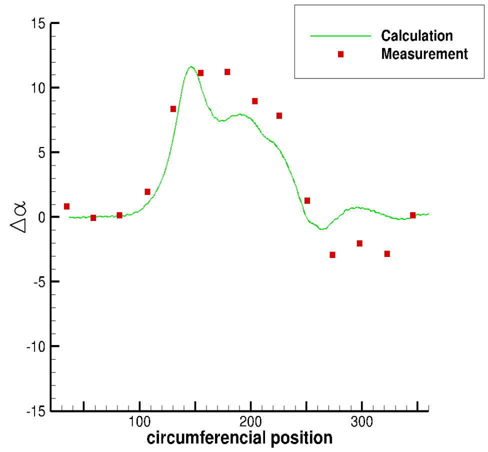

FIGURE 15. CIRCUMFERENCIAL FLOW ANGLE DISTRIBUTION BETWEEN ROTOR AND STATOR, 75% SPAN, (Plane 8)

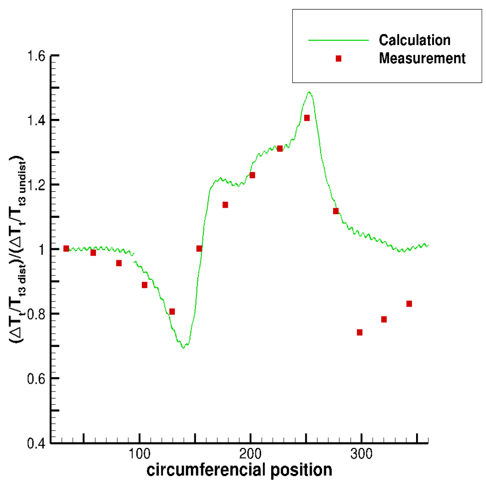

FIGURE 16. CIRCUMFERENCIAL TOTAL TEMPERATURE INCREASE DISTRIBUTION BETWEEN ROTOR AND STATOR, 75% SPAN, (Plane 8)

the measured distortion available. Hence there is no information for radial distortion distribution, which can vary due to possible compressor and distortion grid interaction.

CONCLUSION

Detailed numerical simulations were performed on a transonic compressor stage for uniform and disturbed inflow conditions. For uniform inflow conditions, a comparison between

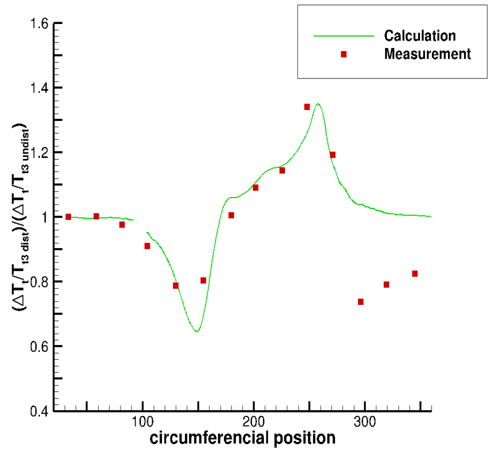

FIGURE 17. CIRCUMFERENCIAL TOTAL TEMPERATURE INCREASE DISTRIBUTION BETWEEN ROTOR AND STATOR, 25% SPAN, (Plane 8)

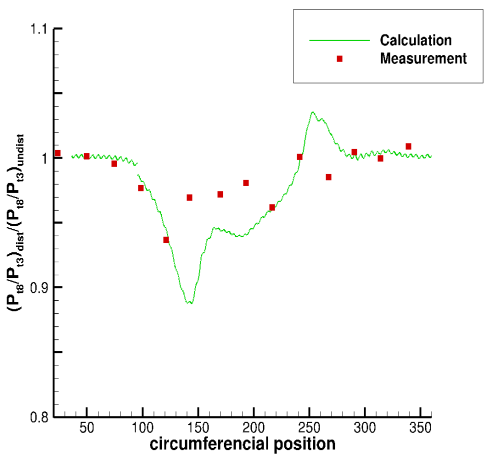

FIGURE 18. CIRCUMFERENCIAL TOTAL PRESSURE INCREASE DISTRIBUTION BETWEEN ROTOR AND STATOR, 75% SPAN, (Plane 8)

predicted and measured flow variables was conducted at different operating conditions. The comparison of circumferentially averaged total temperature profiles indicates that the differences are of an acceptable magnitude. The differences observed are possibly due to the absence of a transition model and therefore an underestimation of the secondary flow effects and profile losses. The simulated Mach number distributions at two different blade heights exhibit a good agreement with the experimental

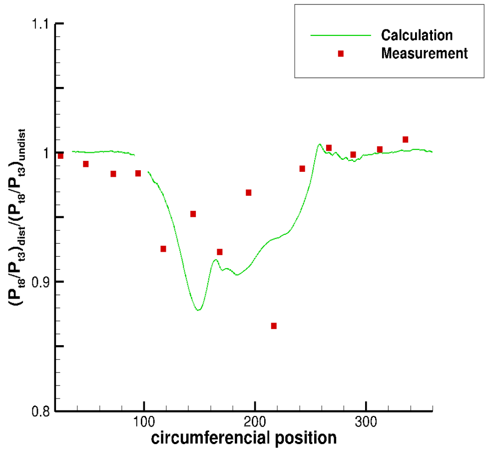

FIGURE 19. CIRCUMFERENCIAL TOTAL PRESSURE INCREASE DISTRIBUTION BETWEEN ROTOR AND STATOR, 25% SPAN, (Plane 8)

data from L2F-measurements. After checking the agreement between simulation and experiment for uniform inflow conditions, numerical simulations with total pressure distortions have been carried out. The results have been presented and discussed in-depth. The numerical calculated and the experimental measured operating point are similar. The results show that general flow trends are well reproduced. For the significant flow quantities the numerical calculation match the trend well. The differences of numerical and measured results at around 300°have been discussed and explained. This work shows that this solver is appropriate for inlet distortion flow calculation. On the follow up, a state-of-the-art compressor rig will be impinged with distorted flow which will be produced by a new designed distortion body. Both the compressor and distortion body flows will be investigated numerically and experimentally. In these investigations the distorted inflow will be modelled directly.

ACKNOWLEDGMENT

The authors gratefully acknowledge the support of the ”Deutsche Forschungsgemeinschaft DFG” (German Research Foundation) which funded this research project and the Leibniz Supercomputing Centre where the calculations were performed.

REFERENCES

[1] Dunker, R., and Hungenberg, H., 1980. “Transonic axial compressor using laser anemometry and unsteady pressure measurements”. Vol. 18, *AIAA Journal*.
[2] Lecht, M., 1983. “Beitrag zum Verhalten von Axialverdichterstufen bei stationärer Störung der Zuströmung”. PhD thesis, RWTH Aachen.
[3] Longley, J., and Greitzer, E., 1992. “Inlet distortion effects in aircraft propulsion system integration”. AGARD-LS-183.
[4] Cousins, W., 2004. “History, philosophy, physics, and future directions of aircraft propulsion system inlet integration.”. ASME Paper GT2004-54210
[5] Schmid N.R., D. L., and Fottner, L., 2000. “Steady performance measurements of a turbofan engine with inlet distortions containing co- and counter-rotating swirl from an intake diffuser for hypersonic flight.”. ASME Paper 2000-GT-11
[6] Reuss, N., 2005. “Untersuchung von kombinierten Eintrittstotaldruckstörungen auf das instationäre Betriebsverhalten eines fünfstufigen Hochdruckverdichters.”. PhD thesis, Universität der Bundeswehr München
[7] Peters, T., and Fottner, L., 2002. “Effects of co- and counter-rotating inlet distortions on a 5-stage hp-compressor.”. ASME Paper 2002-GT-30395
[8] Wadia, 2002. “Forward swept rotor studies in multistage fans with inlet distortion.”. ASME Paper GT-2002-30326.
[9] Wadia, 2008. “High-fidelity numerical analysis of per-rev-type inlet distortion transfer in multistage fans - parti: simulations with selected blade rows.”. ASME Paper GT-2008-50812.
[10] Dunker, R., Strinning, P., and Weyer, H., 1978. “Experimental study of the flow field within a transonic axial compressor rotor by laser velocimetry and comparison with through-flow calculations.”. Vol. 100, *Journal of Eng. For Power*.
[11] Roe, P., 1982. “Approximate Rieman solvers, parameter vectors and difference schemes”. *Journal of Computational Physics*, ***43***.
[12] Wilcox, D., 1998. *Turbulence modeling for CF*. DCW Industries, Anaheim.
[13] Durbin, P. A. Peterson Reif, B. A., 2004. *Statistical Theory and Modeling for Turbulent Flows.* John Wiley & Sons.
[14] Kožulović, D., R. T. K. E., and Nürnberger, D., 2004. “Modifications of a two-equation turbulence model for turbomachinery fluid flows”. Deutscher Luft- und Raumfahrtkongress, Dresden, Germany.
[15] Kožulović, D., 2007. “Modellierung des Grenzschichtumschlags bei Turbomaschinenströmungen unter Berücksichtigung mehrerer Umschlagsarten”. PhD thesis, Ruhr-Universität Bochum, Germany.
[16] Yang, H. Nürnberger, D. W. A., 2002. “A conservative zonal approach with applications to unsteady turbomachinery flows.”. DGLR-JT2002-073, DGLR Jahrestagung, Stuttgart, Germany.
[17] Yang, H., Nürnberger, D., and Kersken, H.-P., 2006. “Toward excellence in turbomachinery computational fluid

dynamics: A hybrid structured-unstructured reynolds-averaged navier-stokes solver.". ASME Journal of Turbomachinery, Vol. 128, pp. 390–402.
[18] Nürnberger, D., 2004. *Implizite Zeitintegration für die Simulation von Turbomaschinenströmungen*. DLR Forschungsbericht 2004-27, Cologne, Germany
[19] Eulitz, F., 2000. "Numerische Simulation und Modellierung der instationären Strömung in Turbomaschinenkomponenten". PhD thesis, Ruhr-Universität Bochum, Germany.
[20] Giles, M., 1991. "A numerical method for the calculation of unsteady flow in turbomachinery". GTL-Report Nr.205, MIT Gas Turbine Laboratory.
[21] Langtry, R. B., 2006. "A correlation-based transition model using local variables for unstructured parallelized cfd codes". PhD thesis, Universität Stuttgart.
[22] Mayle, R. E., 1991. "The role of laminar-turbulent transition in gas turbine engines". ASME Paper 91-GT-261, Orlando, FL.